Journal of Power Sources 193 (2009) 180–184

Contents lists available at ScienceDirect

Journal of Power Sources

journal homepage: www.elsevier.com/locate/jpowsour

Short communication

Anomalous oxide scale formation under exposure of sodium containing gases for solid oxide fuel cell alloy interconnects

Teruhisa Horita*, Haruo Kishimoto, Katsuhiko Yamaji, Manuel E. Brito, Yueping Xiong, Harumi Yokokawa

National Institute of Advanced Industrial Science and Technology (AIST), Japan

ARTICLE INFO

Article history:
Received 19 September 2008
Received in revised form 5 December 2008
Accepted 9 December 2008
Available online 25 December 2008

Keywords:
SOFC
Interconnects
Fe–Cr alloy
Oxide scale
Corrosion

ABSTRACT

Reactivity of oxide scale on Fe–Cr alloy with Na-containing gases was examined to estimate the stability against sodium (Na): vapors of NaCl and Na_2SO_4 exposures with air flow at 1073 K. The identified reaction phases were Cr–Mn spinel, Cr_2O_3, and alloy from the X-ray diffraction of surface with no Na-reaction products. However, the protective oxide scales (Mn–Cr spinel and Cr_2O_3 layers) on the Fe–Cr alloy were partially decomposed by reacting with Na to form Na-compounds inside the oxide scale/alloy interfaces. In some parts, anomalous oxide scales were found around the oxide scale/Fe–Cr alloy interfaces, with forming Na-rich compounds: the compounds were distributed inner parts of oxide scales around oxide scale/alloy interfaces. The stability of oxide scales and degradation were discussed based on the observed distribution of elements.

1. Introduction

In the intermediate operation temperature solid oxide fuel cells (SOFCs), metallic interconnects are one of the important component due to their cost-effectiveness and easy for molding. During operation at 873–1073 K with an exposure to fuel and air, the protective oxide scales can be formed on the Fe–Cr alloy surface. The stability of oxide scales on the alloy interconnects is a key issue for applying alloys as interconnects. Among several candidates, Fe–Cr alloy is one of the promising materials because they can form Cr_2O_3 and Cr–Mn spinel protective oxides layers, which achieve the gas-tightness and relatively high electronic conductivity. So far, a number of reports have been made regarding the stability of oxide scales and Fe–Cr alloys under exposure of fuel cell atmospheres [1–6].

When considering the application of Fe–Cr alloy interconnects in SOFCs near the seashore or marine, we have to consider the effect of sodium (Na) from the sea. It is well known that the alkaline elements can react with Fe–Cr alloy and give a rise to the corrosion on the surface (called as "Hot corrosion") [7–13]. Many reports have been made regarding the corrosion accelerated by salt materials, such as Na_2SO_4. For Ni based alloys, the corrosion behaviors of NiO and Ni were carefully analyzed by Rapp et al. [8,9]. For Fe–Cr alloys (310 stainless steel), significant corrosion behaviors were also reported by coating the $NaCl/Na_2SO_4$ on the alloy surface [13]. NaCl was the main corrosion catalytic specie, and the ratio of $NaCl/Na_2SO_4$ showed the different behaviors of corrosion. About the practical SOFC metallic interconnects, not so much information is available about the Na-corrosion behaviors. The purpose of this study is to clarify the effect of Na vapors on the stability of oxide scales formed on the practical alloy interconnects (ZMG232). Na was supplied to the oxidized Fe–Cr alloy as a gas phase in the high temperature furnace, which was very low concentration compared with the previous study. The formation of Na-containing compounds and the microstructure change of samples were precisely analyzed by using secondary ion mass spectrometry (SIMS) with a sensitive analysis to the Na distributions. The formed compounds and stability of oxide scales were discussed based on the observed data and thermodynamic calculations.

2. Experimental

2.1. Samples and reaction with Na-containing gases

The examined Fe–Cr alloy was the ZMG232, which has been specially developed as interconnects by Hitachi Metals Ltd., Japan. The chemical composition of this alloy is as follows (in mass%); C: 0.02, Si: 0.40, Mn: 0.50, Cr: 22.0, Al: 0.21, Zr: 0.22, La: 0.04, Fe: Balance. The sample surface was polished by a diamond paste to obtain flat and smooth surface prior to the pre-oxidation. The pre-oxidation was performed in air atmosphere at 1073 K for 72 h to form thin

* Corresponding author at: National Institute of Advanced Industrial Science and Technology (AIST), Energy Technology Research Institute, AIST Central 5, Higashi 1-1-1, Tsukuba, Ibaraki 305-8565, Japan. Tel.: +81 29 861 9362; fax: +81 29 861 4540.
E-mail address: t.horita@aist.go.jp (T. Horita).

0378-7753/$ – see front matter © 2008 Elsevier B.V. All rights reserved.
doi:10.1016/j.jpowsour.2008.12.057

protective oxide scale on the Fe–Cr alloy surface. The thickness of oxide scales was about 0.5–1 μm on the surface.

After pre-oxidation, the samples were put into the Al_2O_3 tubes for the reaction with Na-containing gases. Fig. 1 shows schematic drawing of the reactor tube. The sodium (Na) sources are the powders of NaCl and Na_2SO_4 in the Al_2O_3 crucible. Gas flow was made by humidified air (flow rate of 0.05 L min^{-1} and humidification at 30 °C (303 K, $p(O_2) = 0.21$ atm, $p(H_2O) = 0.0422$ atm)). The pre-oxidized Fe–Cr alloy samples were put into the separate Al_2O_3 crucible, whose temperature was controlled at 1073 K. The Na-treatment was examined at 1073 K for 100 h. The position of Na-source crucible is in the inlet of the furnace, where the temperature was a little bit lower than the samples. The evaporated Na components can be delivered to the oxidized alloy sample surface. When the equilibrium is attained between humidified air ($p(O_2) = 0.21$ atm, $p(H_2O) = 0.0422$ atm) and powders of NaCl and Na_2SO_4 with Cr_2O_3, the expected Na vapor pressures are calculated from the thermodynamic database, MALT2/gem (Kagaku Gijutsu-sha, Japan). The calculated vapor pressures of Na-related gas phases at 1073 K are as follows: $p(NaCl(g)) = 9.24 \times 10^{-6}$ atm, $p(NaOH) = 3.25 \times 10^{-9}$ atm, $p(Cl_2(g)) = 5.94 \times 10^{-8}$ atm, $p(HCl(g)) = 2.27 \times 10^{-4}$ atm, $p(Na_2CrO_4) = 1.13 \times 10^{-4}$ atm for NaCl-treatment. For the Na_2SO_4-treatment, the following partial pressures are calculated: $p(Na_2SO_4(g)) = 1.60 \times 10^{-10}$ atm, $p(NaOH) = 3.25 \times 10^{-9}$ atm, $p(SO_2) = 7.51 \times 10^{-9}$ atm, $p(SO_3) = 1.40 \times 10^{-9}$ atm, $p(Na_2CrO_4) = 7.28 \times 10^{-9}$ atm.

2.2. Analysis of Na-treated Fe–Cr alloy

The Na-treated Fe–Cr alloy samples were analyzed by several kinds of analytical methods. The formed phases on the treated alloy surfaces were confirmed by X-ray diffraction (XRD, Rigaku Ultima-III). The microstructures of samples were analyzed by scanning electron microscope (SEM, KEYENCE VE-7800) at surface and oxide scale/alloy interfaces. The elemental distributions were examined by secondary ion mass spectroscopy (SIMS, Cameca ims-5f). We adopted SIMS imaging technique because this is very sensitive to show the distribution of Na around the oxide scale/alloy interfaces. The primary beam was O_2^+ with an accelerating voltage of 12.5 kV. The positive secondary ion (M^+, where M indicates metals) images were measured for different kinds of metals at oxide scales/alloy interfaces.

3. Results

3.1. Surface oxide scale phases and microstructures

The formed oxide scale phases were identified by X-ray diffraction analysis. Fig. 2 shows XRD patterns of Na-treated alloy surface (NaCl and Na_2SO_4 exposures at 1073 K for 100 h). The identified

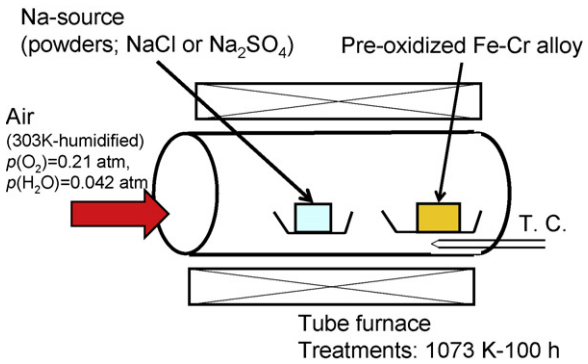

Fig. 1. Schematic diagram of Na-treated reactor.

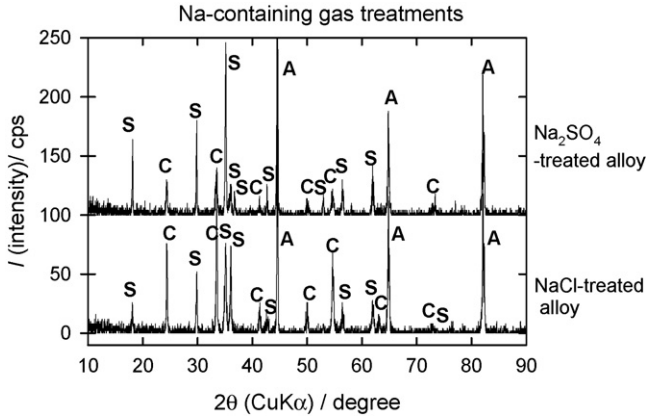

Fig. 2. X-ray diffraction patterns of Na-treated alloys. Upper pattern: Na_2SO_4-treated alloy, bottom pattern: NaCl-treated alloy.

peaks are Fe–Cr alloy (denoted as A), Cr–Mn spinel oxide (denoted as S), and Cr_2O_3 (denoted as C). From the XRD patterns, only oxide scale related phases were identified such as spinel and Cr_2O_3 oxides. No reaction products were identified to the Na-related compounds. This indicates that the amounts of Na-related compounds were very low to detect the conventional XRD analysis.

Fig. 3 shows scanning electron microscope images of air-annealed without Na (a) and Na-treated Fe–Cr alloy surface ((b) and (c)). For air-annealed surface (Fig. 3(a)), small grains were found on the surface. Ridges of grains were observed at the grain boundaries of alloy. On the NaCl-treated surface (Fig. 3(b)), cube or plate shape crystals were observed all the surface of oxidized alloy. This indicates that the formation of second phases on the surface by the reaction of oxide scales with Na-compounds. For Na_2SO_4 treated surface (Fig. 3(c)), grain boundaries of alloy were clearly identified with octahedral shaped crystals. The microstructure of the Na_2SO_4-treated ZMG232 is very similar to the oxidized alloy surface without Na (Fig. 3(a)). These microstructures suggest that NaCl-treatment can affect the reactivity of surface oxide significantly.

3.2. Corrosion by NaCl: microstructures and elemental distribution around the oxide scale/alloy interfaces

Fig. 4 shows microstructures of cross-section at oxide scale/alloy interfaces after NaCl treatments (after the SIMS sputtered surface). The oxide scales are identified as layers on the alloy surface (in Fig. 4(a)). In some parts of oxide scales, we found an anomalous oxide scale close to the oxide scale/alloy interfaces (Fig. 4(b)). This anomalous oxide scale parts are located deep inside the alloy, along the grain boundaries of Fe–Cr alloy. To investigate the distribution of elements around the anomalous oxide scales, SIMS imaging analysis was examined at the interfaces. Fig. 5 shows the distribution of elements by SIMS imaging analysis around the oxide scale/alloy interfaces. It is clear that the higher concentration of Na (high signal counts of Na^+) is identified inside of the oxide scales. From the distribution of Na^+ and Cr^+, the reaction products can be formed by these two elements (such as Na_2CrO_4). However, we have to collect more data to confirm the reaction phases at the anomalous oxide scales. Other parts of the oxide scales, the elemental distributions are almost the same with normal oxide scales. It is the first observation to identify the Na-rich compounds inside the SOFC interconnects.

3.3. Corrosion by Na_2SO_4: microstructures and elemental distribution around the oxide scale/alloy interfaces

Fig. 6 shows SEM images of cross-section around the oxide scale/alloy interfaces. The oxide scales are identified as gray color

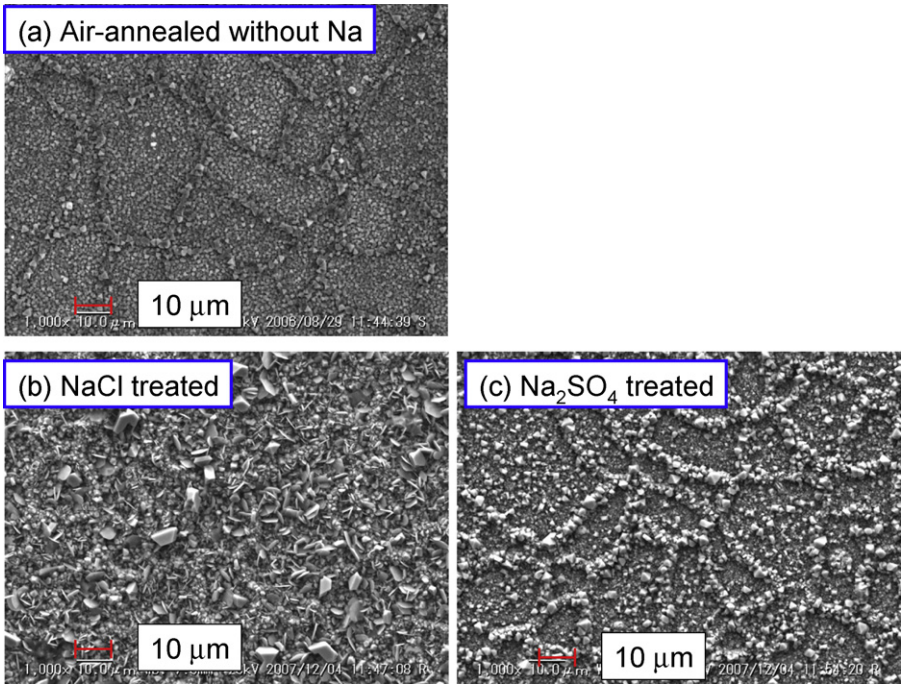

Fig. 3. Scanning electron microscope images of Na-treated Fe–Cr alloy surfaces. (a) Air-annealed without Na (treated at 1073 K for 50 h). (b) NaCl treated Fe–Cr alloy surface (at 1073 K fro 100 h). (c) Na_2SO_4 treated Fe–Cr alloy surface (at 1073 K for 100 h).

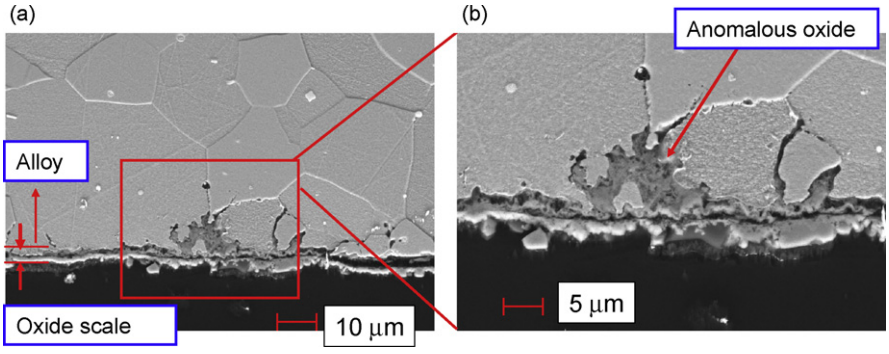

Fig. 4. Scanning electron microscope images of NaCl-treated oxidized Fe–Cr alloy. (a) Low magnification of oxide scale/alloy interfaces. (b) High magnification of anomalous oxide scale part.

parts on Fe–Cr alloy. The oxide scales are composed of octahedron crystals, which are considered to be Cr–Mn spinel or Cr_2O_3. The cross-sectional microstructures are the same with the normal oxide scales. No distinct anomalous oxide scale formation was observed around the oxide scale/alloy interfaces. This is consistent with the surface microstructure observation in Fig. 3(c). Fig. 7 shows the distribution of elements with SIMS imaging analysis corresponding oxide scale/alloy interfaces. The oxide scales are identified as high signal counts of Cr^+ and Mn^+ at the surface region. It is noted that relatively high signal counts of Na^+ is observed at the oxide scale part, which suggests the formation of Na–Cr–Mn reaction products. Even though the supplied vapor pressures of Na are low and the microstructure seems to be normal, some reactions or diffusion of Na can occur at the oxide scale/alloy interfaces.

4. Discussion

4.1. Reactivity of Cr_2O_3 with NaCl and Na_2SO_4

The present results suggest that the protective Cr_2O_3 layer can react with Na-containing gases even in very low Na partial pressures in the gas phase [$p(NaCl) = 9.24 \times 10^{-6}$ atm for the NaCl-treatment and $p(Na_2SO_4) = 1.60 \times 10^{-10}$ atm, $p(NaOH) = 3.25 \times 10^{-9}$ atm for the Na_2SO_4-treatment). When the Na-containing gases can react with Cr_2O_3 and forms Na_2CrO_4, the following reaction can be assumed:

$$2NaCl(g) + 5/4O_2(g) + 1/2Cr_2O_3(s) = Na_2CrO_4(s) + Cl_2(g) \quad (1)$$

$$Na_2SO_4(g) + 1/4O_2(g) + 1/2Cr_2O_3(s) = Na_2CrO_4(s) + SO_2(g) \quad (2)$$

$$2NaOH(g) + 3/4O_2(g) + 1/2Cr_2O_3(s) = Na_2CrO_4(s) + H_2O(g) \quad (3)$$

Since the vapor pressure of Na_2SO_4 is considerably low (1.60×10^{-10} atm), the reactions (1) and (3) can be considered for the reaction with NaCl and Na_2SO_4, respectively. The standard Gibbs energy for the formation of Na_2CrO_4 at 1073 K is -55.792 kJ mol^{-1} for Eq. (1), and -305.211 kJ mol^{-1} for Eq. (3) in the total pressures are assumed to be 1 atm. The equilibrium calculation under very

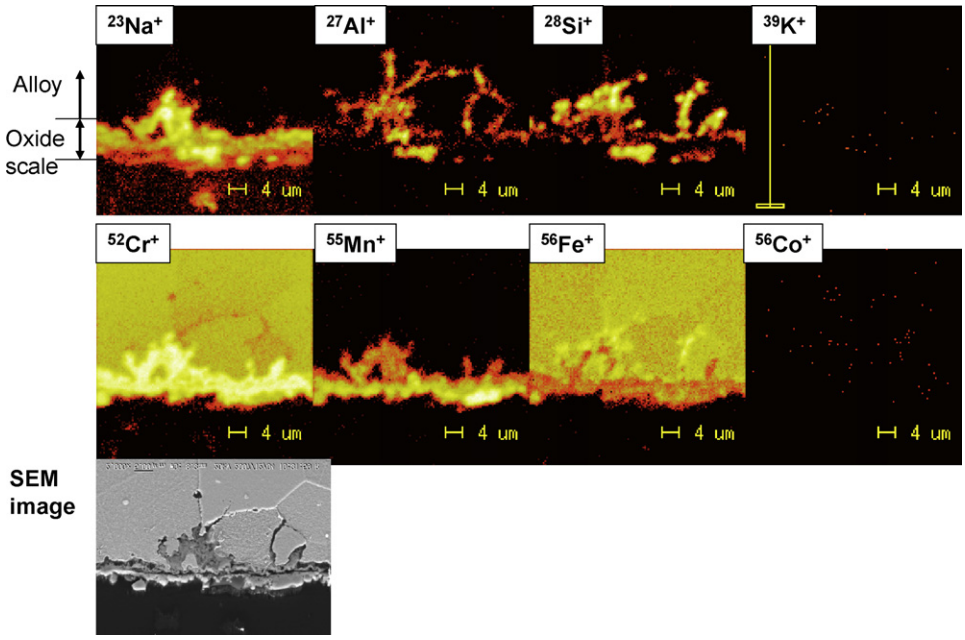

Fig. 5. Secondary ion mass spectrometry (SIMS) images of anomalous oxide scale part (NaCl treated oxidized Fe–Cr alloy).

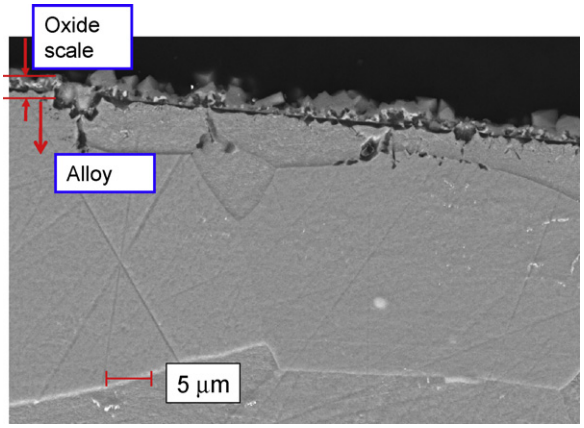

Fig. 6. Scanning electron microscope images of Na_2SO_4-treated oxidized Fe–Cr alloy (cross-sectional images at oxide scale/alloy interfaces).

low Na vapor condition (assuming the experimental condition) suggests that the formation of Na_2CrO_4 can occur by the reaction of NaCl and Na_2SO_4 with Cr_2O_3 from the thermodynamic database, MALT/gem. Thus, the formation of Na_2CrO_4 is expected at the Cr_2O_3 based oxide scales both under Na-containing gases in the experimental condition [8,9]. Under the lower oxygen partial pressures, $NaCrO_2$ can be formed from the equilibrium diagram because of the lower valence of Cr (tri-valence, 3^+) [14]. The effects of Cl_2 and SO_2 should be also considered in Eqs. (1) and (2). Recently, Haga et al. [15] have reported that the effect of gases containing S and Cl on the Ni anode performances in SOFCs. Some effects should be considered from these gases (such as SO_2 and Cl_2) though the partial pressures of these gases are very low in this study. The precise analysis of these gases on the stability of Cr_2O_3 will be made in the future work.

In the present observation, the distribution of Na is found at the inside of the oxide scale, suggesting a fast diffusion of Na in Cr_2O_3 or high reactivity of Na with Cr_2O_3. The formation of Na-compounds at the oxide scale/alloy interfaces has been reported in the real stack using the similar Fe–Cr alloy interconnects [16]. Although the present study does not use the glass seal materials,

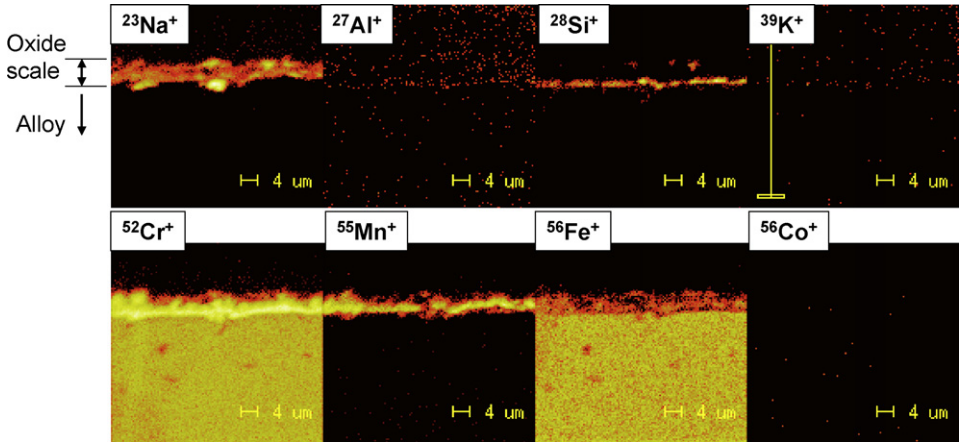

Fig. 7. Secondary ion mass spectrometry (SIMS) images of oxide scale/alloy interfaces treated in Na_2SO_4.

Na vapors coming from NaCl and Na_2SO_4 powers can be significant for the reaction with Cr_2O_3. The concentration level of Na in the previous study was reported to be about 50 ppm [16]. When Eq. (1) is in equilibrium condition, the concentration level of Na_2CrO_4 is above 10 ppm, which is expected to be the same levels of the previous study. Although there is not so much data regarding the concentration of sodium (Na) in air, the concentration levels of Na^+ ions in rain water is above 1 mg per litter (about ppm) [17]. The concentration levels of Na in air atmosphere is expected to be lower than that of Na^+ in rain water.

4.2. Anomalous oxide scale formation

In Figs. 3 and 4, the oxide scales were partially decomposed and Na-compounds were found in the deep inside the oxide scales. In this part, the oxide scales are completely different from the normal oxide scales on the Fe–Cr alloy. The breakdown of protective oxide could occur by the reaction of Eq. (1). The anomalous oxide scale formation is significant in the NaCl-treatment. Once Na_2CrO_4 is formed, a eutectic can be formed in the NaCl–Na_2CrO_4 mixtures. The melting point of NaCl–Na_2CrO_4 eutectic is about 628 °C (901 K) [13], which suggests the promotion of surface reaction. The difference in the surface microstructures (Fig. 3) can suggest the formation of eutectic in the NaCl–Na_2CrO_4 mixtures.

5. Conclusion

Reactivity of oxide scales of Fe–Cr alloy with Na-containing gases was examined to estimate the stability against sodium (Na): vapors of NaCl and Na_2SO_4 with air flow were examined at 1073 K. The identified reaction phases were Cr–Mn spinel, Cr_2O_3, and alloy from the X-ray diffraction of surface. No apparent reaction products were identified from the XRD patterns. However, the protective oxide scales (Mn–Cr spinel and Cr_2O_3 layers) on the Fe–Cr alloy were partially decomposed by reacting of Na with Cr_2O_3 to form Na-compounds inside the oxide scale/alloy interfaces. In some parts, anomalous oxide scales were found around the oxide scale/Fe–Cr alloy interfaces. The equilibrium calculations were examined to estimate the reaction products and long-term stability. The formation of Na–Cr–O compounds and a eutectic are expected, which will affect the stability of Cr_2O_3 based protective oxide scales.

Acknowledgements

Part of this work was supported by the New Energy Development Organization (NEDO) under the SOFC system development project. The authors are very grateful to the organization.

References

[1] H.U. Anderson, F. Tietz, in: S.C. Singhal, K. Kendall (Eds.), Interconnects in High Temperature Solid Oxide Fuel Cells, Elsevier, 2003, pp. 173–195 (Chapter 7).
[4] A. Toji, T. Uehara, Extended abstract of 14th SOFC Symposium, The SOFC Society of Japan, Tokyo, 2005, p. 60.
[5] T. Horita, Y. Xiong, K. Yamaji, N. Sakai, H. Yokokawa, J. Power Sources 118 (2003) 35–43.
[6] T. Horita, Y. Xiong, H. Kishimoto, K. Yamaji, N. Sakai, H. Yokokawa, J. Power Sources, 131 (2004) 293–298.
[7] D.N.H. Trafford, D.P. Whittle, Corros. Sci. 20 (1980) 509–530.
[8] N. Otsuka, A. Rapp, J. Electrochem. Soc. 137 (1990) 46–52.
[9] R.A. Rapp, Corros. Sci. 44 (2002) 209–221.
[10] C.L. Zhang, Y. Niu, W.T. Wu, J.Q. Zhang, F. Gesmundo, J.T. Guo, Solid State Ionics 63–65 (1993) 672–677.
[11] C.L. Zeng, J. Li, Electrochim. Acta 50 (2005) 5533–5538.
[12] Y. Xi, J. Lu, Z. Wang, L. He, H. Wang, Trans. Nonferrous Met. Soc. China 16 (2006) 511–516.
[13] C.-C. Tsaur, J.C. Rock, C.-J. Wang, Y.-H. Su, Mater. Chem. Phys. 89 (2005) 445–453.
[14] Phase Equilibria Diagrams Volume XIII, Figure 10317, The American Ceramic Society-NIST, 2001.
[15] K. Haga, S. Adachi, Y. Shiratori, K. Itoh, K. Sasaki, Solid State Ionics 179 (2008) 1427–1431.
[16] K. Ogasawara, H. Kameda, Y. Matsuzaki, T. Sakurai, T. Uehara, A. Toji, N. Sakai, K. Yamaji, T. Horita, H. Yokokawa, J. Electrochem. Soc. 154 (7) (2007) B657–B663.
[17] Report of the chemical compositions from rain in 2005, Japan Meteorological Agency (in Japanese), http://www.data.kishou.go.jp/obs-env/cdrom/report2005/html/5_1.htm.